Available online at www.sciencedirect.com
SCIENCE DIRECT®
Journal of Power Sources 119–121 (2003) 69–75
JOURNAL OF POWER SOURCES
www.elsevier.com/locate/jpowsour

# A new lithium–copper–iron-oxide as a negative electrode material for lithium-ion batteries

Sung-Kyun Chang, Hyeong-Jin Kim, Seung-Tae Hong*

*Battery R&D, LG CHEM Research Park, Taejon 305-380, South Korea*

**Abstract**

Synthesis, crystal structure and electrochemical reactivity of $Li_3CuFe_3O_7$ in a lithium (Li) cell are reported as a new material for the first time. The crystal structure is γ-$LiFeO_2$ type, and the chemical formula can be re-written as $(Li_{0.714}Cu_{0.286})$ $(Li_{0.143}Fe_{0.857})O_2$. The average charge–discharge voltages versus Li are 1.75/0.9 V, which indicates the material may be used as a negative electrode in Li-ion batteries. The material demonstrates a discharge capacity of up to 970 mAh/g, but shows also a significant irreversible capacity of >250 mAh/g. It decomposes to very small particles of lithium oxide and unidentified species during the first discharge. The reversibility is strongly dependent on *C*-rate, electrode composition, initial particle sizes and/or crystallinity, implying that a better electrochemical performance may be achieved by adjusting these parameters. The observation of higher than theoretical capacity (694 mAh/g) for the reversible reaction of $Li_3CuFe_3O_7 + 11Li \leftrightarrow 7Li_2O + Cu + 3Fe$, however, suggests the possibility that the Li–M (Cu, Fe) alloy formation–decomposition process is involved.


*Keywords:* Lithium copper iron oxide; γ-$LiFeO_2$ type; Lithium-ion batteries; Negative electrode materials; Combinatorial chemistry; Exploratory synthesis

## 1. Introduction

In a search for new negative electrode materials for lithium-ion (Li-ion) batteries to replace carbonaceous materials with respect to its limited capacity of <370 mAh/g in commercial systems and its low density, alternative systems such as lithium titanates [1–3], vanadates [4], amorphous composite tin oxides [5], and composite alloys [6,7] have been extensively studied. Recently 3d-transition metal oxides have received particular attention because of their large reversible capacities as high as 700 mAh/g with a 100% capacity retention up to 100 cycles and high rates [8–10]. It was also suggested that the reversible reactivity mechanism to transition metal oxides towards lithium totally differs from the classical one based either on reversible intercalation of lithium into host structures or on Li alloying reactions.

Exploratory synthesis [11], or combinatorial chemistry, in the search for new compounds, crystal structures, and properties is an important aspect of materials chemistry, leading to a discovery of a large variety of new phases, sometimes unexpected or unforeseen. We have been looking for new electrode materials, especially focused on complex transition metal oxides of Li–M1–M2–O systems (M1, M2 = transition metals), by means of the exploratory synthetic approach.

In this report, we present a novel oxide $Li_3CuFe_3O_7$ discovered for the first time during the exploratory synthesis searching for new electrode materials in Li–Cu–Fe–O system.

## 2. Experimental

$Li_3CuFe_3O_7$ was first discovered as a single phase during the exploratory synthesis in Li–Cu–Fe–O system. It was first synthesized by conventional solid-state reaction from appropriate molar ratio of $Li_2O$, CuO, and $Fe_2O_3$ at 900 °C for 10 h in air. It was also synthesized by a sol–gel route from lithium hydroxide, copper and iron nitrates and citric acid. Samples were characterized by X-ray diffraction (XRD) using a Rigaku Powder X-ray diffractometer equipped with Cu Kα radiation. Crystal structure was determined by X-ray Rietveld refinement technique using GSAS program [12]. Electrochemical performance was characterized with a coin type cell versus lithium metal. The positive electrodes were made from active material, graphitic carbon (KS-6) as a conductive additive, and poly(vinylidene difluoride) (PVdF) as a binder with various compositions of (40:53:7),

* Corresponding author. Tel.: +82-42-866-2498; fax: +82-42-863-2934.
*E-mail address:* sthong@lgchem.com (S.-T. Hong).

0378-7753/03/$ – see front matter © 2003 Elsevier Science B.V. All rights reserved.
doi:10.1016/S0378-7753(03)00128-9

(60:33:7), and (80:13:7), which were coated on Cu-foils. The electrolyte used was 1 M $LiPF_6$ in EC:EMC (1:2 by volume). The cell was assembled in a glove box under argon with <1 ppm $H_2O$. Electrochemical study was carried out with TOSCAT-3100U controller system (Toyo, Japan) in galvanostatic mode with various rates (0.2*C*, 0.1*C*, 0.02*C*, 1*C* = 700 mAh/g) up to 20 cycles between 0.3 and 2.8 V.

## 3. Results and discussion

### 3.1. Structural analysis

The powder X-Ray diffraction pattern for single phase $Li_3CuFe_3O_7$ showed that the crystal structure is γ-$LiFeO_2$ type [13] in which the cations are ordered so that the structure is tetragonally distorted from the cubic rock-salt type structure of α-$LiFeO_2$ [14]. The unit-cell structure is shown in Fig. 1, where the ordered arrangement of Li-site (M1) and Fe-site (M2) are shown clearly. The positions of γ-$LiFeO_2$ were used as starting values in the Rietveld refinement. After successive refinements of the peak profile parameters, of the occupancy of Li, Cu, and Fe ions, of the positional parameters for oxygen, and lastly of the overall thermal parameter, the *R*-values were lowered to: $R_{wp} = 0.88\%$, $R_p = 1.31\%$, $\chi^2 = 0.28$. In order to refine the occupancies of metal ions in each site, Cu ion was first set to be the same as Fe in the beginning of the refinement because of their similar X-ray atomic scattering factors. Then a constraint was applied so that the atomic ratio between Li versus transition metals are 3:4, and Li-ions were assumed to be mixed with transition metal ions in each site of M1 and M2. It was very interesting to see the transition metal occupancies in M1 and M2 sites are 1:3 ratio which is the same as the Cu:Fe ratio of the sample. Then the refinement was continued with a reasonable assumption that the transition metals are Cu and Fe in M1 and M2 sites, respectively. Structural parameters, the final atomic coordinates and occupancies and thermal parameters are summarized in Tables 1 and 2. The most important bond distances and angles are calculated in Table 3. The observed, calculated, and difference profiles are shown in Fig. 2. It is obvious that the M1 site is tetragonally distorted octahedral one as can be seen from the distance difference between the elongated axial ones (2.479 Å) and the other four planar ones (2.042 Å). The M2 site is relatively undistorted octahedral one: the distances are 1.973 and 2.042 Å, respectively. The ordering of M1 and M2 sites in the structure seems to come from the difference of $Cu^{2+}$ ($d^9$, Jahn–Teller ion) and $Fe^{3+}$ ($d^5$) ion in their electronic configurations.

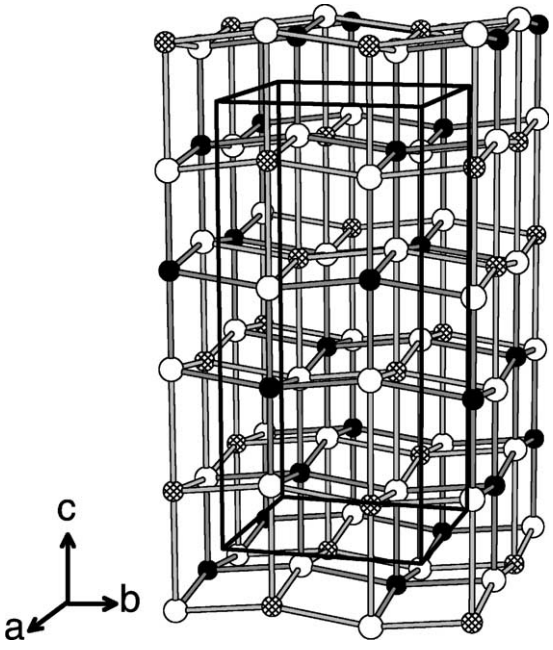


Fig. 1. Crystal structure of $Li_3CuFe_3O_7$ with γ-$LiFeO_2$ type structure. Ordered arrangement of Li-site (M1) and Fe-site (M2) are shown: open sphere = oxygen, hatched sphere = M1 ($Li_{0.71}Cu_{0.29}$), black sphere = M2 ($Li_{0.14}Fe_{0.86}$). Unit cell is shown by dark solid lines.

Table 1
Crystal data for $Li_3CuFe_3O_7$ at room temperature

| | |
|---|---|
| Formula | $(Li_{0.714}Cu_{0.286})(Li_{0.143}Fe_{0.857})O_2 = Li_3CuFe_3O_7$ |
| Formula weight | 121.30 |
| Crystal system | Tetragonal |
| Space group | $I4_1/amd$ (no. 141) |
| Unit-cell dimensions (at 298 K), *z* | $a = b = 4.0521(3)$ Å, $c = 8.9045(7)$ Å, $z = 4$ |
| Cell volume (Å$^3$) | 146.21(2) |
| Density, calculated (g/cm$^3$) | 4.723 |
| $R_p$ (%) | 1.31 |
| $R_{wp}$ (%) | 0.88 |
| $\chi^2$ | 0.2804 |

Table 2
Atomic coordinates and thermal parameters for $Li_3CuFe_3O_7$ at room temperature with standard deviation in parentheses

| Atom | Wyck | *x* | *y* | *z* | Fraction |
|---|---|---|---|---|---|
| Li1 | 4a | 0 | 1/4 | 7/8 | 0.717(3) |
| Cu | 4a | 0 | 1/4 | 7/8 | 0.283(3) |
| Li2 | 4b | 0 | 1/4 | 3/8 | 0.141(3) |
| Fe | 4b | 0 | 1/4 | 3/8 | 0.859(3) |
| O | 8e | 0 | 1/4 | 0.5966(9) | 1.0 |

$100U_{iso} = 2.10(13)$.

Table 3
Selected bond distances (Å) and angles (°) for $Li_3CuFe_3O_7$

| | | | |
|---|---|---|---|
| M1–O × 2 | 2.479(8) | O–M1–O | 165.8(4) |
| M1–O × 4 | 2.0418(10) | | 90.88(5) |
| M2–O × 2 | 1.973(8) | O–M2–O | 180.0(0) |
| M2–O × 4 | 2.0418(10) | | 97.1(2) |
| M1–M2 × 6 | 2.8653(2) | | 90.88(5) |
| M1–M2 × 6 | 3.0101(2) | | 82.9(2) |

(Li1, Cu) ≡ M1, (Li2, Fe) ≡ M2.

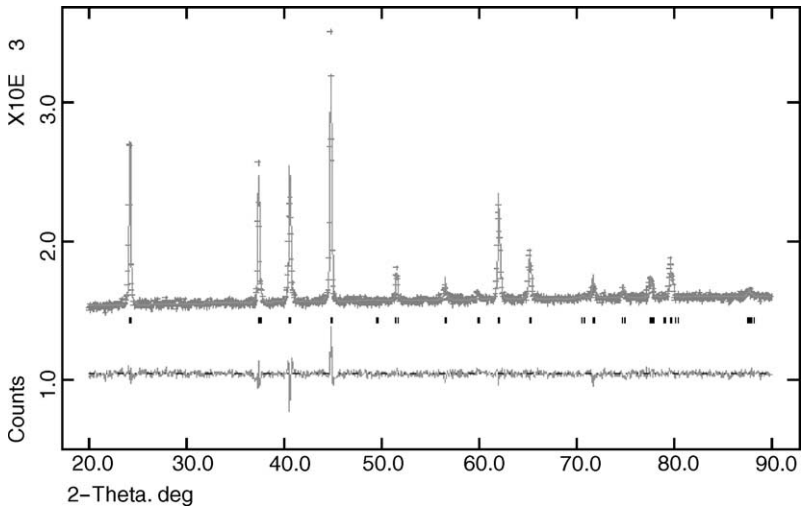


Fig. 2. Observed and calculated powder X-ray (Cu Kα) diffraction pattern for $Li_3CuFe_3O_7$. Below the observed data (crossed) and calculated (solid line) pattern, the difference plot is shown. Vertical lines indicate the Bragg reflection positions.

### 3.2. Electrochemical characteristics of $Li_3CuFe_3O_7$

Galvanostatic charge–discharge curves and capacity fading are shown in Fig. 3 for *C*-rates of 0.2*C*, 0.1*C*, and 0.02*C*. The curves show a similarity to those observed from MO/Li cells with Co, Ni or Fe oxide [8]. During the first discharge, the potential drops rapidly to a plateau at 0.9 V, and then continuously decreases down to cut-off voltage, 0.3 V. The discharge capacities at the end of the plateau and at the cut-off voltage at 0.02*C* rate are 700 and 970 mAh/g, respectively. When charged, the cell showed a plateau around 1.75 V, and a capacity of 720 mAh/g. Note that

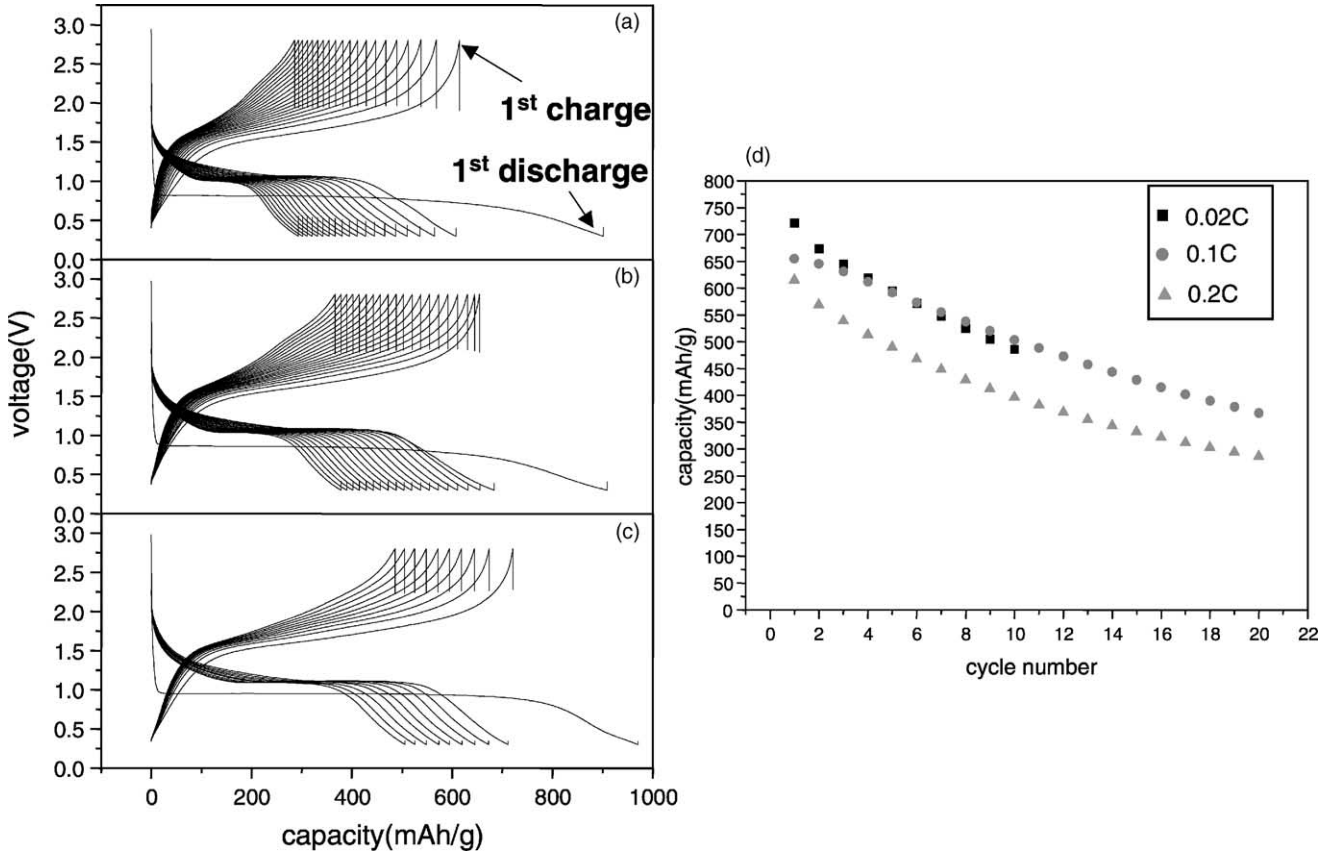


Fig. 3. Charge–discharge curves of $Li_3CuFe_3O_7$|1 M $LiPF_6$ in EC:EMC (1:2)|Li cell in galvanostatic mode at room temperature at various rates: (a) 0.2*C*; (b) 0.1*C*; (c) 0.02*C*; and (d) capacity fading (1*C* = 700 mAh) ($Li_3CuFe_3O_7$:KS-6:PVdF = 40:53:7, voltage window: 0.3–2.8 V).

the first-cycle capacity loss was about ca. 25%, but the capacity loss after the first cycle was decreased significantly. The loss was higher with higher *C*-rates. It should be also noted that the capacity from the second cycle is still about twice as much as those for typical carbonaceous materials (330–350 mAh/g), while exhibiting a double density. The reversible capacity of the cells, however, continuously decayed on cycling. The second discharge curve differs considerably from the first, suggesting a quite different structural modification between lithium and the electrode material.

Since $Li_3CuFe_3O_7$ has very poor electronic conductivity, a relatively larger amount of conducting carbon is necessary when an electrode is made. The amount of the conducting additive could be an important parameter for the material to react with Li in the cell. Electrode composition dependence of charge–discharge curves is shown in Fig. 4 where three different electrode compositions of $Li_3CuFe_3O_7$:KS-6:PVdF are tested. It is evident that the larger amount of conducting carbon is included in the electrode, the higher is the capacity of the cell, as expected. It also leads to a better capacity retention during cycling.

It was reported that the ability to retain the capacity of copper oxide-based Li cells was found to be strongly dependent on the particle size [8,15]. In order to study the effects of particle size or morphology on the capacity retention on cycling, we produced the materials from different synthetic routes such as conventional solid-state reaction, sol–gel process, and ball-mill treatment of the materials from solid-state reaction. The X-ray diffraction patterns for each product are shown in Fig. 5. The compound from solid-state reaction showed the sharpest peaks with lowest background, indicating the best crystallinity.

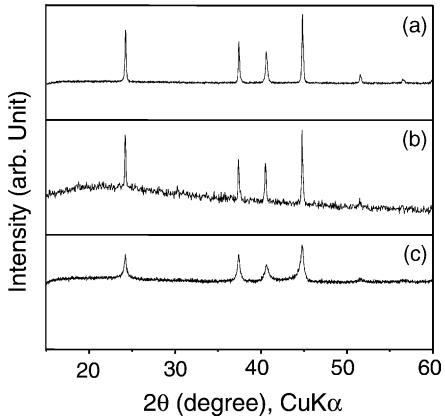


Fig. 5. X-ray diffraction patterns of $Li_3CuFe_3O_7$ from different synthetic routes: (a) conventional solid-state; (b) sol–gel; (c) ball-mill.

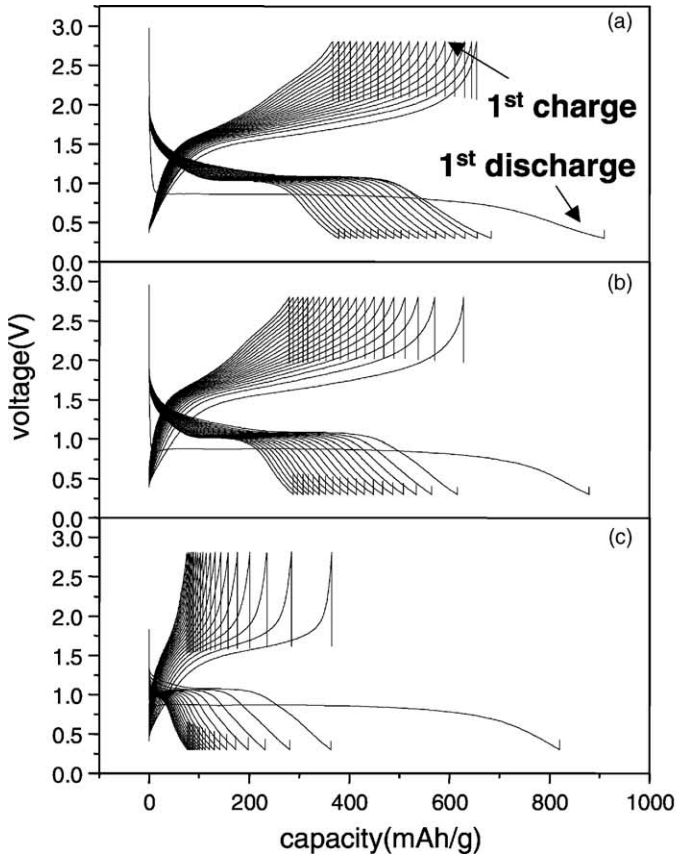


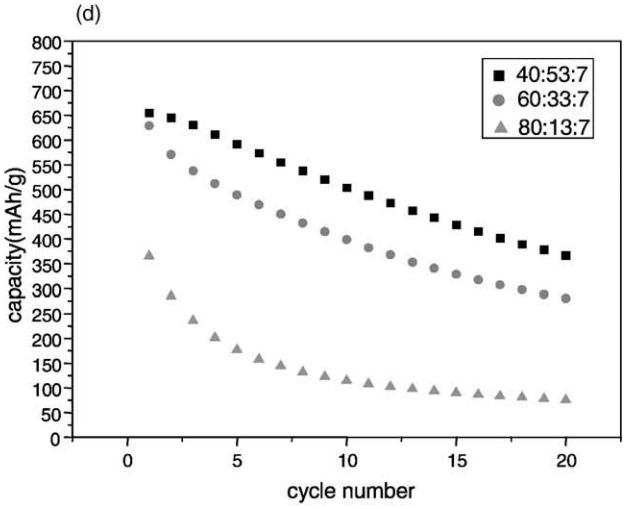


Fig. 4. Charge–discharge curves of $Li_3CuFe_3O_7$|1 M $LiPF_6$ in EC:EMC (1:2)|Li cell in galvanostatic mode at room temperature with various electrode compositions of $Li_3CuFe_3O_7$:KS-6:PVdF: (a) 40:53:7; (b) 60:33:7; (c) 80:13:7; and (d) capacity fading (0.1*C* rate, voltage window: 0.3–2.8 V).

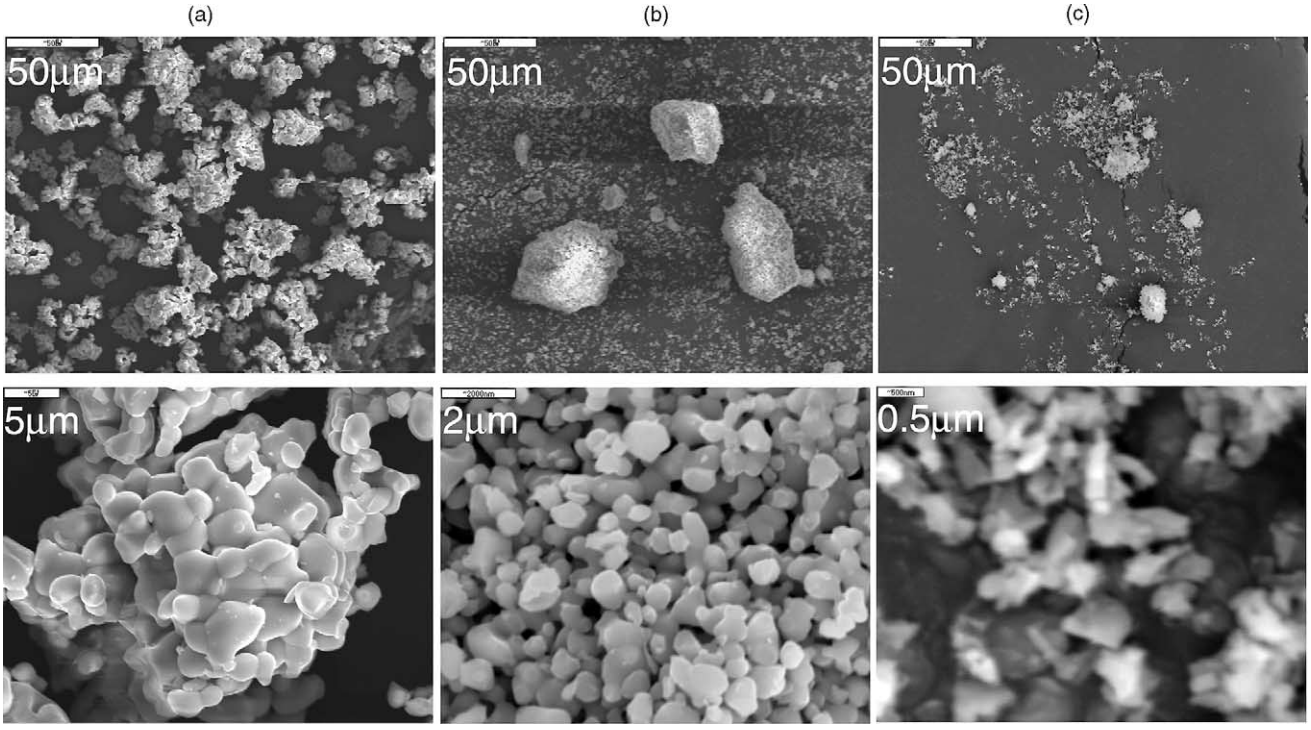


Fig. 6. SEMs of $Li_3CuFe_3O_7$ powders from different synthetic routes: (a) conventional solid-state; (b) sol–gel; (c) ball-mill.

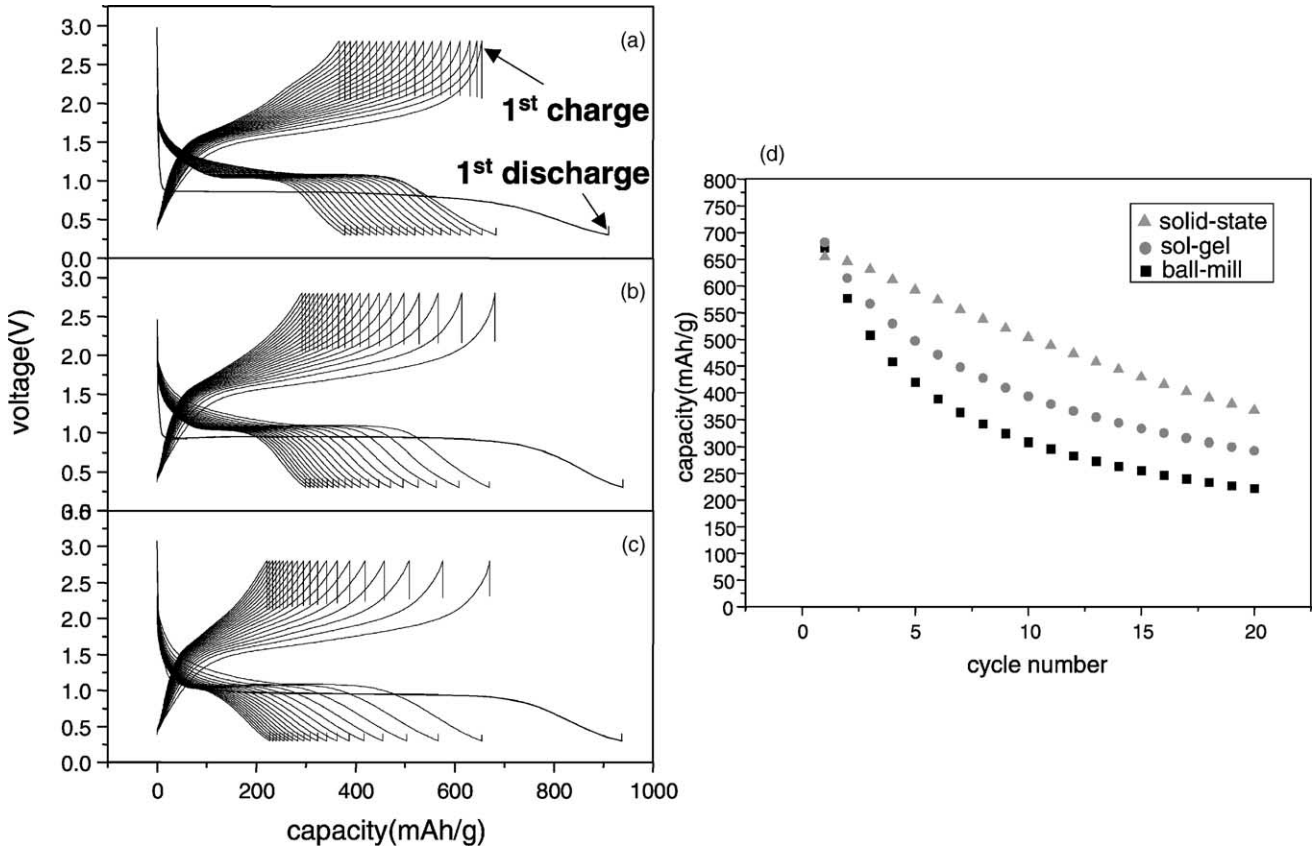


Fig. 7. Charge–discharge curves of $Li_3CuFe_3O_7$|1 M $LiPF_6$ in EC:EMC (1:2)|Li cell in galvanostatic mode at room temperature with $Li_3CuFe_3O_7$ from different synthetic routes: (a) conventional solid-state; (b) sol–gel; (c) ball-mill; and (d) capacity fading (0.1*C* rate, $Li_3CuFe_3O_7$:KS-6:PVdF = 40:53:7, voltage window: 0.3–2.8 V).

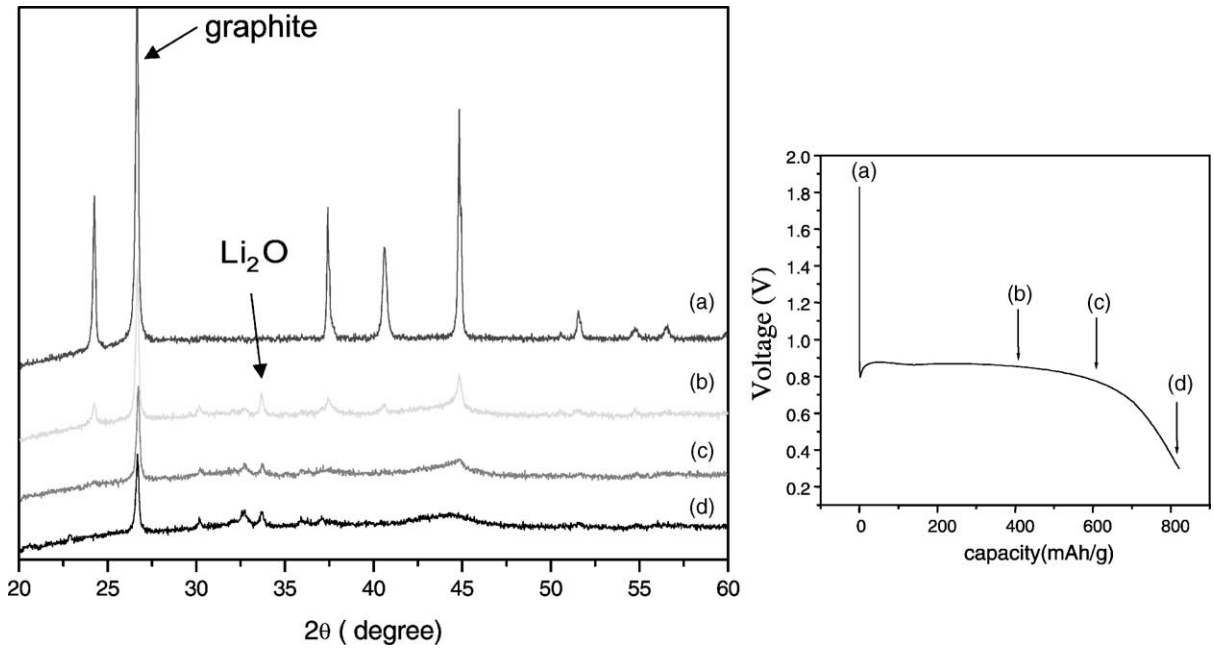


Fig. 8. Ex-situ XRD patterns of $Li_3CuFe_3O_7$ electrodes collected at various stages of discharge of a $Li_3CuFe_3O_7$|1 M $LiPF_6$ in EC:EMC (1:2)|Li cell. The right figure shows the first discharge profile for the cell with the letters denoting at which the corresponding XRD patterns were taken.

The ball-milled materials showed relatively wide peaks, indicating the smallest particle sizes, while the materials from sol–gel showed intermediate characteristics. The particle sizes are examined by scanning electron microscopes (SEMs) as shown in Fig. 6. The aggregations of the small particles are seen in the top photos of Fig. 6. The particle sizes are on the order of ~5 μm, <1 μm and ⩽0.5 μm for the materials from solid-state (a), sol–gel (b), and ball-mill (c), respectively. The particle sizes of ball-milled material were too small for our SEM resolution. The charge–discharge curves for $Li_3CuFe_3O_7$/Li cells with three different sizes of $Li_3CuFe_3O_7$, and capacity fading are shown in Fig. 7. The larger particle sizes (up to ~5 μm in our experiment) showed better capacity retention on cycling.

Since $Li_3CuFe_3O_7$ is a close-packed structure, as shown in Fig. 1, there is no available space for extra Li-ion insertion. The electrochemical reaction in the Li/$Li_3CuFe_3O_7$ cell must differ from the well-known intercalation reaction in which the crystal structure of the host material is retained during Li insertion/desertion. In order to study the mechanism of the reaction, ex-situ X-ray diffraction patterns of $Li_3CuFe_3O_7$ electrodes were collected at various stages of discharge of the cell (Fig. 8). The first discharge profile for the cell is also shown in the right with the letters denoting at which the corresponding XRD patterns were taken. As Li reacted with $Li_3CuFe_3O_7$, we observed a continuous decrease in the $Li_3CuFe_3O_7$ Bragg peaks that totally vanishes at full discharge, leading to an amorphous-like pattern except for the small and wide peaks corresponding $Li_2O$ and some unidentified phases which should be reduced species of copper and iron elements or compounds. When the coin cell was disassembled after discharge, it was also apparent that the volume of the electrode was increased considerably. The theoretical capacity for the following reaction is 694 mAh/g as suggested in other transition metal oxide [8]:

$$Li_3CuFe_3O_7 + 11Li \leftrightarrow 7Li_2O + Cu + 3Fe \quad (1)$$

The higher capacity of the first discharge, however, implies a further reduction below zero oxidation of metal species, suggesting a possibility of involving Li–M (Cu, Fe) alloying process together with the above reaction. Further work is required to determine the exact structural transformations that occur during the discharge and charge of $Li_3CuFe_3O_7$ electrodes.

## 4. Conclusion

Here, we report a new complex oxide $Li_3CuFe_3O_7$, a possible candidate for negative electrode materials in lithium batteries. The great advantages of transition metal oxides-based lithium-ion cells over current commercial $LiCoO_2$/carbon cells may be the fact that these materials exhibit about twice the reversible capacity as carbon per unit mass, and two to three times its density, thus four to six times the capacity of carbon per unit volume. But there are the sacrifice in the cell voltage (~2 V instead of 4 V), and the initial irreversible capacity problem to overcome. Even though CoO showed an excellent capacity retention up to more than 100 cycles [8], $Li_3CuFe_3O_7$ exhibited a significant capacity fading. The reversibility, however, seems to depend strongly on *C*-rate, electrode composition and/or initial particle sizes or crystallinity. Therefore, there still remains

works to do for optimizing the materials itself and/or electrode compositions to achieve better electrochemical performance.

## Acknowledgements

We thank Eun-Young Goh, Seungdon Choi and Jeong-Ju Cho for their helpful discussions.

## References

[1] S. Garnier, C. Bohnke, O. Bohnke, J.L. Fourquet, Solid State Ionics 83 (1996) 323.
[2] R.K.B. Goves, J.R. Tolchard, H. Tukamoto, T. Murai, J.S. Irvine, J. Electrochem. Soc. 146 (1999) 4348.
[3] T. Ohzuku, A. Ueda, N. Yamamoto, J. Electrochem. Soc. 142 (1995) 1431.
[4] E. Baudrin, S. Laruelle, S. Denis, M. Touboul, J.-M. Tarascon, Solid State Ionics 123 (1999) 139.
[5] Y. Idota, T. Kubota, A. Matsufuji, Y. Maekawa, T. Miyasaka, Science 276 (1997) 1395.
[6] O. Mao, R.A. Dunlap, J.R. Dahn, J. Electrochem. Soc. 146 (1999) 405.
[7] K.D. Kepler, J.T. Vaughey, M.M. Thackeray, Electrochem. Solid-State Lett. 2 (1999) 307.
[8] P. Poizot, S. Laruelle, S. Grugeon, L. Dupont, J.-M. Tarascon, Nature 407 (2000) 496.
[9] P. Poizot, S. Laruelle, S. Grugeon, L. Dupont, J.-M. Tarascon, J. Power Sources 97–98 (2001) 235.
[10] F. Badway, I. Plitz, S. Grugeon, S. Laruelle, M. Dolle, A.S. Gozdz, J.-M. Tarascon, Electrochem. Solid-State Lett. 5 (2002) A115.
[11] J.D. Corbett, Inorg. Chem. 39 (2000) 5178.
[12] A.C. Larson, R.B. Von Dreele, General Structure Analysis System, Report no. LAUR086-748, Los Alamos National Laboratory, Los Alamos, NM 87545.
[13] D.E. Cox, W.J. Takei, G. Shirane, Am. Crystallogr. Assoc.: Program Abst. 1962 (1962) L6.
[14] J.C. Anderson, M. Schaefer, J. Phys. Chem. Solids 25 (1964) 961.
[15] S. Grugeon, S. Laruelle, R. Herrera-Urbina, L. Dupont, P. Poizot, J.-M. Tarascon, J. Electrochem. Soc. 148 (2001) A285.